Int. J. Electrochem. Sci., 14 **(2019)** 9633 – 9646, doi: 10.20964/2019.10.05

International Journal of
ELECTROCHEMICAL
SCIENCE
www.electrochemsci.org

Acceleration Effects of Hydroxylamine Sulfate on Electroless Gold Plating on Ni–Pd Surfaces

Wenjuan Yao, Daoxin Wu[*]*, Zhongliang Xiao, Yiwei Wang, Ronghua Yang*

School of Chemistry and Food Engineering, Changsha University of Science and Technology, Changsha, 410114, China
[*]E-mail: daoxinwu@126.com

Received: 9 June 2019 / *Accepted:* 24 July 2019 / *Published:* 30 August 2019

Hydroxylamine sulfate (HAS) was used to accelerate Au deposition following the covering of a Ni–Pd substrate with Au layer. The influence of HAS on the electroless gold plating bath and deposition procedure was investigated. The acceleration mechanism, nucleation mechanism, and corrosion resistance were analyzed via electrochemical methods. The surface microtopography and the chemical and phase compositions of Au layers were also characterized. Results showed that HAS did not affect the stability of the plating bath because of the reaction of cyanide and hydroxylamine. HAS also positively accelerated Au deposition due to its excellent catalyzed oxidation on the Au surface. As the optimum concentration, 0.02 M HAS increased the deposition rate by 70%. At the same deposition time, the transformation of the nucleation model increased the size of Au grains and smoothened the surface of the Au layer after the addition of 0.02 M HAS.

Keywords: electroless gold plating, electrochemical methods, HAS, nucleation mechanism

1. INTRODUCTION

To prevent corrosion during exposed copper metallization and providing a solderable surface [1], final finishes [2-5] must be established on the surface of printed circuit boards (PCBs); these final finishes include electroless nickel (EN) [6], electroless nickel/immersion gold (ENIG) [7,8], electroless nickel/electroless palladium/immersion gold (ENEPIG) [9,13], immersion tin (I-Sn) [10], immersion silver (I-Ag) [11], and organic solderability preservatives [12].

ENEPIG, as the solution to the "black pad" defect, is a modification of the conventional ENIG finish [13, 14] and is capable of supporting a good soldering surface and gold wire bondable surface [15, 16]. The Pd layer, which is located between Ni and Au layers, can suppress the growth of Ni oxides and the migration of Ni/Au [14]. Hence, increasing the thickness of the Au layer requires the addition of a

reducing agent to the EG plating bath [17]; examples of reducing agents include hydrazine, dimethylamine borane (DMAB), thiourea, sodium thiosulfate, ascorbic acid, and sodium hypophosphite (SHP) [18-22].

Sulfite and thiosulfate are frequently used as reducing agents in electroless gold plating, and they have been reported in many studies [7,8,17,19]. The main advantage of sulfite and thiosulfate is that they can serve as reducing agents in gold plating bath and as complexing agents, which help maintain the stability of gold plating bath. However, S and Au are co-deposited during deposition, as described in detail in the work of Li [8], and S deteriorates the welding performance of the Au layer [23].

SHP has been systematically studied [24-28] as a common reducing agent in electroless plating. Delaunois [26] studied autocatalytic electroless nickel plating, and Mardilovich [27] studied autocatalytic electroless palladium plating with SHP as the reducing agent; however, pure gold does not catalyze the oxidation of SHP, and the EG plating process is hindered after the Au layer covers the Ni–Pd surface, as described in Vorobyova's study [28]. SHP can suppress the precipitation of the substrate in electroless gold plating because of its catalyzed oxidation by the Ni–Pd surface, and it does not influence the welding performance of the plating layer.

In recent years, hydroxylamine has been frequently used to prepare Au nanoparticles, which can effectively increase the size of nanomaterials as a surface-catalyzed reducing agent [29-33]. In the current work, HAS was applied to solve the hard Au deposition following Ni–Pd coverage when only SHP is used. The results showed that HAS can greatly improve the Au deposition rate without affecting the stability of the gold plating bath. Hence, the effects of HAS on the plating process and Au layer were systematically studied, and the molecular model of Au^+ coordinates was analyzed using Materials Studio (MS). Furthermore, the influences of HAS on nucleation and growth and the corrosion resistance of layers were investigated using electrochemical methods and scanning electron spectrometry(SEM).

2. EXPERIMENTAL

2.1 Sample preparation

Copper sheets (10mm × 10mm × 0.2mm) were used as substrates in this study. Before electroless gold (EG) plating, the Cu substrate underwent pretreatment and EN and EP plating successively. The pretreatment included washing and activation of the surface to obtain 3–4 μm Ni layer in the EN plating bath and then 0.07–0.1 μm Pd layer in the EP plating bath. The copper sheet covered with Ni–Pd was immersed in the EG plating bath. The composition and operating conditions of the EG plating bath are shown in Table 1. All reagents were of analytical grade, and all solutions were prepared using distilled water.

Table 1. Composition and operating conditions of EG plating bath

Contents	Concertration(g/L)	condition
Au^+	0.5	
$C_6H_{17}N_3O_7$	20	
SHP	16	
ATMP	10	
EDTA-2Na	5	
$TPSO_3$	0.01	
pH		6.0
Temperature		95℃
Deposition time		10 min

2.2 Characterization

The stability of the EG bath with different reducing agents was examined using a heat test (10 H, 90 ℃). A UV spectrophotometer (TU-1902) was used to reflect the coordination between HAS and Au^+. X-ray fluorescence (XRF-2000) was used to measure the thickness of the layers in a fast and non-destructive way. The surface morphology of the Au layer was determined using SEM (JEOL-7600F). The phase compositions and crystal structure of the layer were analyzed via X-ray diffraction (D/Max 2500 PC Rigaku).

All electrochemical measurements were carried out on a CHI760D electrochemical workstation. The saturated calomel electrode and saturated mercurous sulfate electrode (SMSE) were used as reference electrodes, and a platinum electrode was used as the counter electrode. The pure Au electrode was used as the working electrode in cyclic voltammetry (CV) and chronopotentiometry, which can describe the catalytic oxidation of HAS on the Au surface. The Ni–Pd–Au-coated copper was used as the working electrode in the electrochemical impedance spectroscopy (EIS) test to determine the charge transfer performance on the plated surface following the covering of Ni–Pd with the Au layer. The Ni–Pd-coated copper was used as the working electrode in the open circuit potential (OCP) test, which can reveal the electrochemical properties during gold plating. In chrono amperes, the Ni–Pd-coated copper was used as the working electrode, and the overpotential was set to −1.0 V versus SMSE. This method is commonly used to study the effects on nucleation during plating. The Ni-, Ni–Pd-, and Ni–Pd–Au-coated copper samples were used in the Tafel test to show the corrosion resistance of the Au layer.

The molecular model of Au^+ coordinates was built in the MS workspace. The DMol3 program incorporated in the MS computational package was employed for this study. The Fukui function and orbital calculations were performed using the LDA–PWC potential functional in conjunction with the DND basis set. The charge was set to −1 for symmetry. Optics calculations were performed using the LDA–PWC potential function in conjunction with the DNP basis set. The charge was set to −1 for symmetry, solvent set water (dielectric constant is 78.54) use COSMO.

3. RESULTS AND DISCUSSION

3.1 Effects of HAS on electroless gold plating bath

Figure 1(a) shows the effects of the different reducing agents on the stability of the plating bath after 10 h of heating at 90 ℃. The bath turned yellow and produced some black precipitate after the addition of VC. Some black precipitates also appeared after the addition of DMAB. The plating bath contained SHP and became unstable when added with small amounts of other reducing agents. When HAS was added to the bath, no damage was observed. Moreover, HAS preferentially reduced Au^+ onto existing Au structures as opposed to self-nucleating as a surface-catalyzed reducing agent [32, 33]. Figure 1(b) shows the UV spectra of 0.01 M HAS, 0.1 M HAS, 0.01 M $AuK(CN)_2$, and their mixture. The 0.01 M and 0.1 M HAS had an absorption peak at 190 nm, which corresponded to $–NH_2OH$. Meanwhile, 0.01 M $KAu(CN)_2$ had five peaks at approximately 195, 210, 220, 260, and 280 nm because the hydrolysis of −CN produced $−NH_2$, −COOH, and −C=O. After the addition of 0.01 M HAS to the $KAu(CN)_2$ solution, the absorption peak was enhanced in the range of 190–210 nm. When HAS was added to 0.1 M, the absorption peaks were continuously enhanced, and a redshift occurred. These observed phenomena could be related to the reaction of cyanide and hydroxylamine, as shown in reaction (I), and revealed that amidoxime groups can provide better gold adsorption characteristics than cyanide [34].

$$CN^- + NH_2OH \rightarrow C(NH_2)NOH^- \qquad \text{Reaction (I)}$$

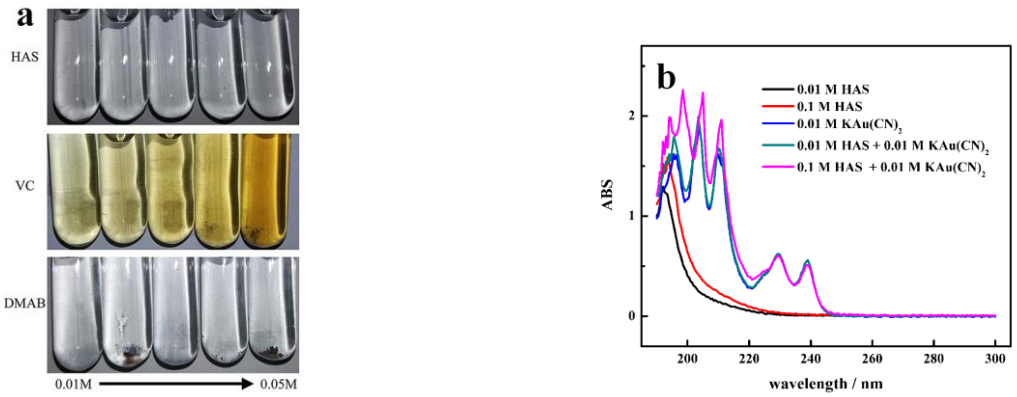

Figure 1. a) effects of HAS, VC and DMAB on thermal stability of electroless gold plating bath. b) UV spectrum of 0.1 M HAS, 0.01 M $AuK(CN)_2$ and their mixture.

3.2 Effects of HAS on the thickness and deposition rate of Au layer

Figure 2(a) shows the thickness of the Au layer deposited after 10 min given different concentrations of HAS. The thickness increased with the addition of HAS and then decreased after more than 0.02 M HAS was added. The possible reason was the right shift of reaction I with the addition of HAS. In addition, a large amount of amidoxime groups shielded the activity of Au^+[34]. Figure 2(b) shows the deposition rates given the reducing agents 0.15 M SHP and the mixture of 0.15 M SHP and

0.02 M HAS. The deposition rate was fast in the initial stage and then slowed down after the Ni–Pd surface was covered by Au. This trend became intense when only 0.15 M SHP was used. Obviously, the deposition rate with complex reducing agents was faster than that with 0.15 M SHP as the reducing agent in any stage, and 0.02 M HAS increased the deposition rate by 70%.

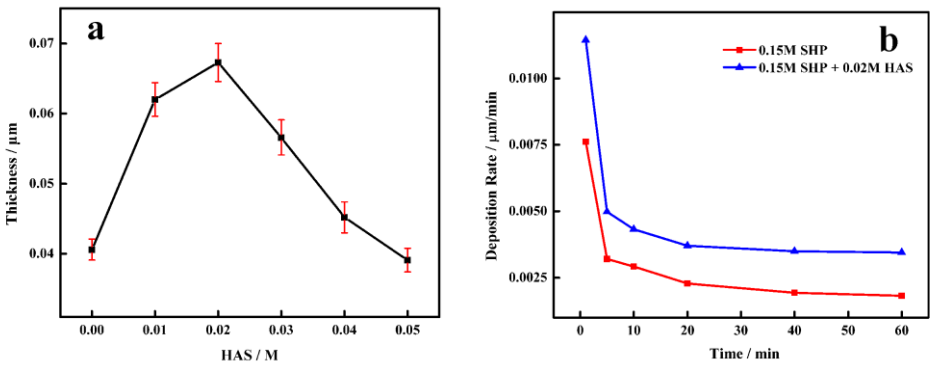

Figure 2. a) Au thickness after 10min electroless plating in EG plating bath a without and with different concentrations of HAS, b) deposition rate as reducing agent respectively is 0.15 M SHP.

3.3 Analysis of Molecular Model

Figure 3 shows the molecular models of $Au(CN)_2^-$ and $Au(C(NH_2)NOH)_2^-$ after geometric optimization. The Fukui function plays an important role in the study of chemical reactivity and selectivity [35]. Local softness was calculated according to Equation (I), and the global nucleophilic attack orientation was compared across different molecules; the results are listed in Table 2. The values of the Fukui function calculated using two different analysis methods indicated that the reactivity of the Au atom decreased in $Au(C(NH_2)NOH)_2^-$. Thus, Au^+, which coordinated with amidoxime, was more difficult to reduce than cyanide.

$$S_r = f_r \times S \approx f_r/\Delta E_{lumo\text{-}homo} \qquad \text{Equation (I)}$$

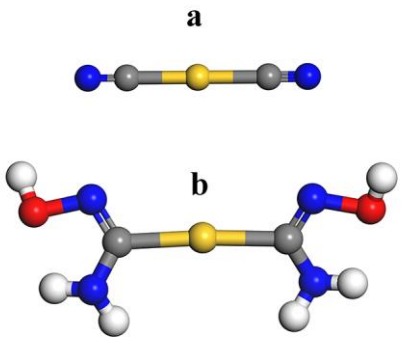

Figure 3. molecular model after geometric optimization, a) $Au(CN)_2^-$, b) $Au(C(NH_2)NOH)_2^-$.

To evaluate the energy behavior of $Au(CN)_2^-$ and $Au(C(NH_2)NOH)_2^-$, we calculated the highest occupied molecular orbital(HOMO) energy and the lowest unoccupied molecular orbital (LUMO) energy, as shown in Figure 4(a). Reaction (I) indicated that $Au(C(NH_2)NOH)_2^-$ was more capable of donating electrons and less capable of obtaining electrons than $Au(CN)_2^-$, resulting in the high E_{Homo} of $Au(CN)_2^-$ and lower E_{Lumo} of $Au(C(NH_2)NOH)_2^-$.

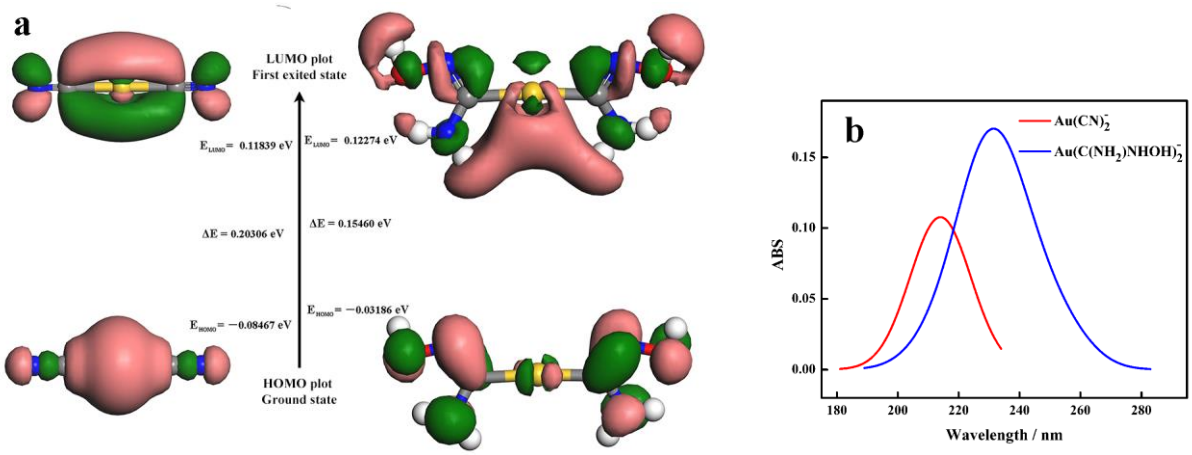

Figure 4. a) atomic orbital HOMO – LUMO composition of the frontier molecular orbital of $Au(CN)_2^-$ and $Au(C(NH_2)NOH)_2^-$, b) calculated UV spectrum of $Au(CN)_2^-$ and $Au(C(NH_2)NOH)_2^-$.

The larger energy gap (ΔE) of $Au(CN)_2^-$ indicated better stability and worse optical properties than $Au(C(NH_2)NOH)_2^-$, and only the right shift of reaction (I) could improve the stability of $Au(C(NH_2)NOH)_2^-$. The calculated UV spectrum is shown in Figure 4(b). The characteristic absorption peak of $Au(C(NH_2)NOH)_2^-$ had stronger ABS and bigger wavelength than $Au(CN)_2^-$. Accordingly, the absorption peak was enhanced and shifted to a long wavelength when $Au(CN)_2^-$ turned to $Au(C(NH_2)NOH)_2^-$, as observed in Figure 1(b). According to the analysis of the coordinates' molecular structure, an unstable but low reaction activity $Au(C(NH_2)NOH)_2^-$ was transformed from $Au(CN)_2^-$, and this unstable coordinate became stable, thus decreasing the reactivity of Au^+ at high HAS concentrations.

Table 2. The values of calculated Fukui function of $Au(CN)_2^-$ and $Au(C(NH_2)NOH)_2^-$.

Detail	Mulliken			Hirshfeld		
	f^+	f^-	f^0	f^+	f^-	f^0
$Au(CN)_2^-$	0.623	0.401	0.512	0.524	0.370	0.447
$Au(C(NH_2)NOH)_2^-$	0.148	0.180	0.164	0.104	0.172	0.138

3.4 Electrochemical Analysis

Figure 5(a) shows the OCP–time curves of the EG plating process at different concentrations of HAS in the EG plating bath. Apparently, all curves had the same tendency, and the potential increased

with the EG process and then became relatively stable when the reaction reached equilibrium [7, 8]. However, plateau potential had a positive shift when HAS existed in the EG plating bath, indicating that the thickness of the Au layer increased after the addition of HAS, and the degree of shift varied with the different concentrations of HAS. A 150s' potential was considered as the plateau potential (inset of Figure 3(a)), and its trend was variable, similar to the thickness changes in Figure 2(a). The 0.02 M HAS had the best acceleration in EG plating.

Figure 5(b) shows the EIS spectra, and Table 2 lists the electrochemical parameters after fitting by the equivalent circuit. The charge transfer resistance (R_{ct}) revealed the charge transfer performance on the plated surface in EG plating. The better this capability is, the better the deionization tendency of the plated surface will be. Table 3 shows that R_{ct} and polarization resistance (R_p) decreased after HAS was added, and the oxidation of HAS on the Au surface led to a high charge transfer. However, at a HAS concentration above 0.02 M, the coordination between $C(NH_2)NOH^-$ and Au^+ prevented Au^+ from receiving electrons. Hence, R_p remained stable. These findings prove that HAS continued to accelerate during EG plating after Ni–Pd was completely covered by Au. Moreover, 0.02 M HAS was found to be the best choice. These results are similar to those of the OCP–time test and thickness detection.

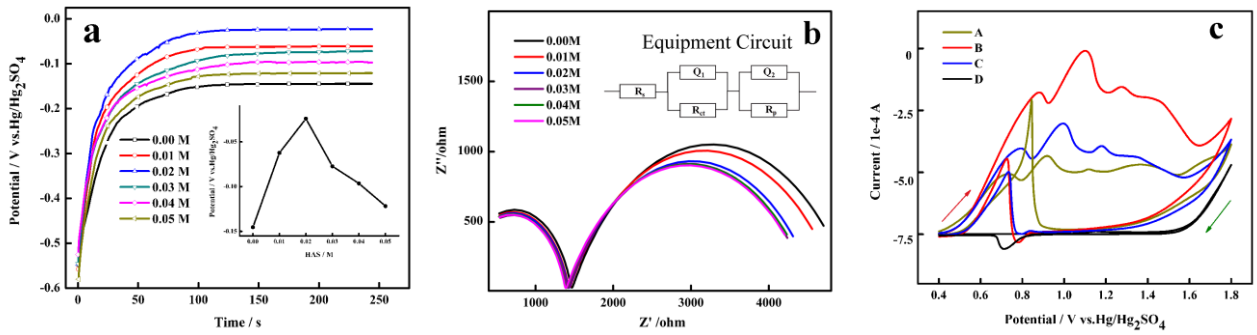

Figure 5. a) Open circuit potential-time curves of EG process with different concentrations of HAS, inset: I vs. M at 150s, b) Nyquist plots of the copper covered Ni-Pd-Au exposed to EG bath with different concentrations of HAS, c) CV of 0.02 M HAS and 0.02 M H_2SO_4, A: 0.02 M HAS, scan rate is 0.01 V/s, B: 0.02 M HAS, scan rate is 0.05 V/s, C: 0.02 M HAS, scan rate is 0.1 V/s, D: 0.02 M H_2SO_4, scan rate is 0.1 V/s.

To confirm the oxidation of HAS on the Au surface, we showed the CVs of 0.02 M HAS and 0.02 M H_2SO_4 in Figure 5(c). A cathodic peak above 0.7 V appeared and was associated with the formation of Au oxide layer on the electrode surface [28]. At a scan rate of 0.1 V/s, H_2SO_4 had no response in the anodic area, but HAS had some oxidation peaks above 0.7–1.4 V at all scan rates. This finding indicated that HAS undergoes excellent catalyzed oxidation on the Au surface and that the oxidation was carried out step by step, which is consistent with the description of Shimada [36]. Therefore, the mechanism of HAS was presumed, as shown in Figure 6. HAS, as an autocatalytic reducing agent, can also react with cyanide, thus ensuring the stability of the plating solution but limiting the amount of HAS. HAS was accelerated as soon as Au grain formed and remained after the Ni–Pd surface was completely covered by the Au layer.

Table 3. Electrochemical parameters obtained by fitting the equivalent circuit

Name	R_s (Ω cm^2)	Q_1 $Y/\Omega^{-1}\cdot cm^{-2}\cdot sn$	n	R_{ct} (Ω cm^2)	Q_2 $Y/\Omega^{-1}\cdot cm^{-2}\cdot sn$	n	R_p (Ω cm^2)
0.00 M	4.003×10^{-5}	1.590×10^{-9}	0.8607	1461	1.384×10^{-4}	0.6718	3610
0.01 M	6.275×10^{-5}	1.636×10^{-9}	0.8583	1427	7.089×10^{-5}	0.6678	3481
0.02 M	1.510×10^{-4}	1.804×10^{-9}	0.8519	1422	7.337×10^{-5}	0.6736	3190
0.03 M	2.764×10^{-5}	2.212×10^{-9}	0.8387	1416	7.650×10^{-5}	0.6765	3111
0.04 M	4.836×10^{-6}	1.617×10^{-9}	0.8603	1388	7.840×10^{-5}	0.6653	3167
0.05 M	2.509×10^{-7}	1.678×10^{-9}	0.857	1384	7.941×10^{-5}	0.6641	3144

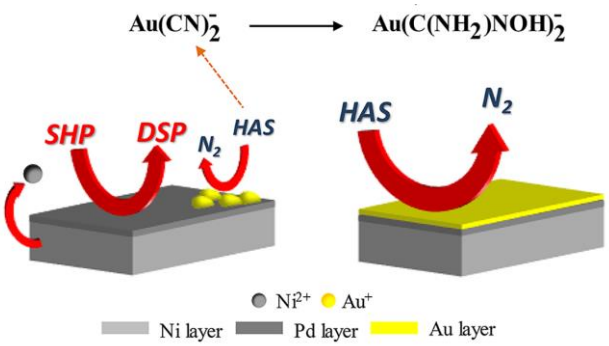

Figure 6. Reaction schematic of HAS on plating bath and plated surface.

3.5 Nucleation mechanism

The nucleation and growth information can be deduced from the corresponding potentiostatic current transients [37]. Chronoamperometry was employed during electroless gold plating on the Ni–Pd surface. The I–t curves are shown in Figure 7(a) after deducting the charging current of the electric double layer. These curves indicated a common trend in which the current density increased dramatically along with the formation of the nucleus and the growth of the new phase. Then, the current density decreased and stabilized because the diffusion was controlled on the plated surface after the maximum value was reached. The peak diffusion current density (I_m) increased after the addition of HAS, with that under 0.02 M HAS being higher than that under 0.05 M HAS. The deposition rate was the fastest with 0.02 M HAS. Hence, the diffusion current density had a positive shift.

The nucleation model can usually be determined on the basis of the linear relationship of the I/t^n curves, and the 3D nucleation process can be derived using the diffusion-controlled growth model at n=1/2 or 3/2. Thus, when n = 1/2, a significant I–$t^{1/2}$ linear relationship can be found (inset of Figure 7(a)). The 3D nucleation mechanism can be established using the Scharifker–Hills model. All current

transients can be presented in a non-dimensional form by plotting the normalized current $(I/\mathrm{Im})^2$ versus time (t/tm). The comparison between $(I/\mathrm{Im})^2/(t/\mathrm{tm})$ curves and two theoretical curves, namely, instantaneous and progressive nucleation, was used to determine the nucleation mechanism, as shown in Figure 7(b). The instantaneous nucleation and theoretical nucleation curves were calculated using Equations (II) and (III), respectively. Under instant nucleation, the growth rate of the nucleus was fast, and the deposition rate was faster. Under continuous nucleation generated by the new nucleus, the Au layer was uniform, and the deposition rate was slow. In comparison with 0.00 M and 0.05 M HAS, 0.02 M HAS changed the nucleation mode, and the trend gradually changed from instantaneous nucleation to continuous nucleation interval. This transition was related to the change in deposition rate.

$$(I/I_m)^2=1.9542\left(1-\exp\left(-1.2564(t/t_m)\right)\right)^2/(t/t_m) \qquad \text{Equation (II)}$$

$$(I/I_m)^2=1.2254\left(1-\exp\left(-2.3367(t/t_m)\right)\right)^2/(t/t_m) \qquad \text{Equation (Ⅲ)}$$

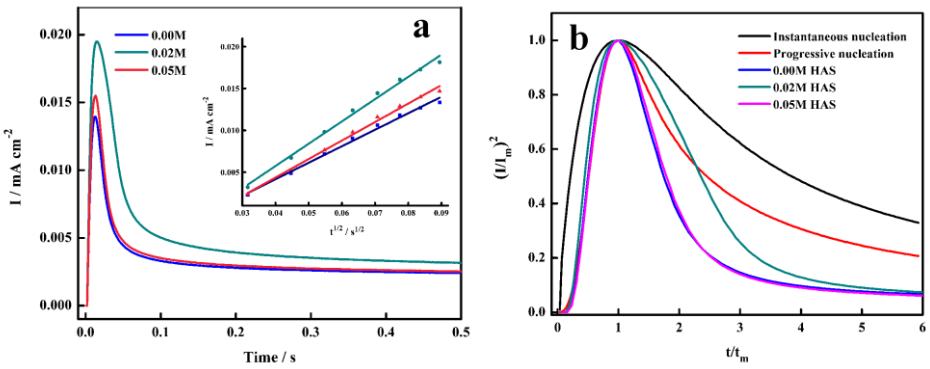

Figure 7. SEM of Au surface after 10min electroless plating in EG plating bath with different concentrations of HAS.

3.6 Micromorphology Analysis

Figure 8 shows the SEM of Au layers deposited after 10 min with different concentrations of HAS. The Ni–Pd surface was completely covered by Au, and the micromorphology was different at various concentrations of HAS[30]. The size of the Au grain increased first and then decreased with the addition of HAS. The size of the Au grain was the largest, and it appeared to fuse with the addition of 0.02 M HAS. Before the Ni–Pd surface was completely covered by the Au layer, the nucleation growth tended to be in the instantaneous nucleation mode with 0.02 M HAS. A high growth rate of nucleation resulted in a large Au grain.

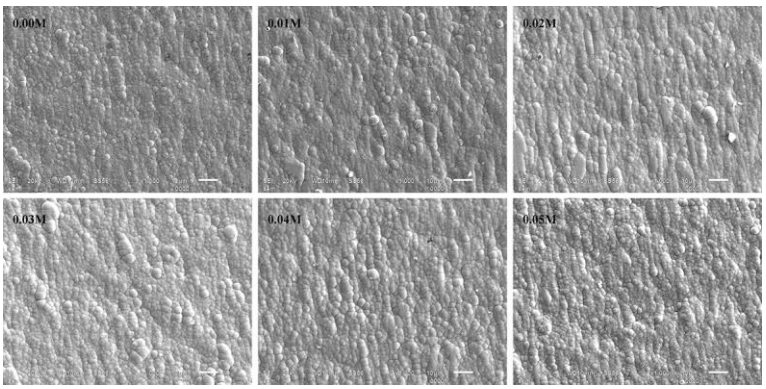

Figure 8. potentiostatic current transients during EG plating on Ni-Pd surface, inset: I vs. $t^{1/2}$ plots of the rising parts of the current transients, b) Non-dimensional plots of $(I/Im)^2$ vs. t/tm for the current transients.

The SEMs of the Au layer deposited with 0.15 M SHP and the mixture of 0.15 M SHP and 0.02 M HAS were compared, as shown in Figure 9. In general, the size of the Au grain increased, and the surface of the Au layer became smooth with time. After 5 min of deposition, no difference was observed between 0.15 M SHP and the complex reducing reagents, but the Au grain was bigger with the complex reducing reagents than with only 0.15 M SHP after 10 min. After more than 20 min, nucleation growth indicated continuous nucleation because of the decrease of the deposition rate, but the smoothening of the Au surface was especially obvious because of the acceleration of HAS during Au deposition.

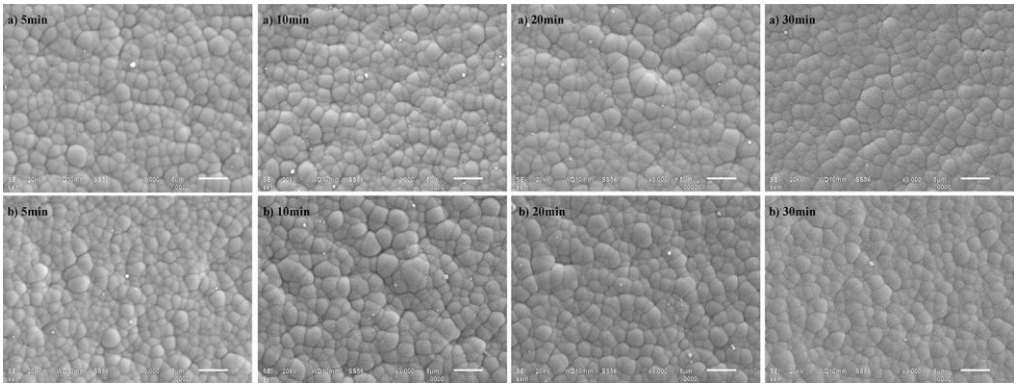

Figure 9. SEM of Au surface after electroless plating in EG plating bath, a) 0.15 M SHP, b) 0.15 M SHP and 0.02 M HAS.

Figure 10 shows the surface microtopography and cross-sectional microtopography of the Ni–Pd surface after the Au layer was removed. No Ni corrosion problem occurred on the Ni–Pd substrate after EG plating because the catalytic oxidation of SHP on Ni and Pd can prevent the precipitation of Ni. Moreover, the addition of HAS did not cause substrate corrosion.

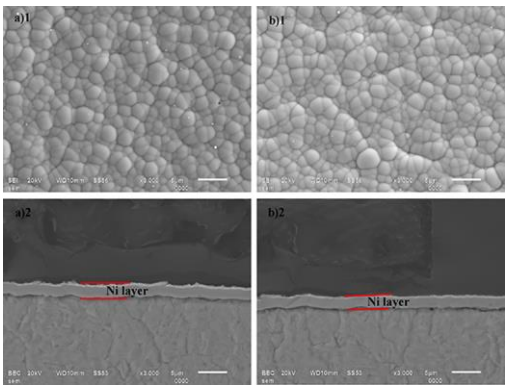

Figure 10. Surface microtopography and cross-sectional microtopography of Ni-Pd surface after EG plating, a) 0.15 M SHP, b) 0.15 M SHP and 0.02 M HAS.

3.7 Chemical Element Analysis

The chemical component of the Au surface was analyzed via EDS, and the changes of Au and O mass with different concentrations of HAS are shown in Figure 11(a). The variable trend of Au mass was coincident with that shown in Figure 2(a) as the thickness of Au increased. However, O mass decreased with the addition of HAS partly because Au increased. However, the oxidizing reaction was suppressed because the oxidation of HAS can be catalyzed by the Au surface[27].

The XRD patterns of the Au layer deposited with 0.15 M SHP and the mixture of 0.15 M SHP and 0.02 M HAS are shown in Figure 11(b). No obvious change was observed in the crystalline phase after 0.02 M HAS was added. Three peaks of Cu (111), Cu (200), and Cu (220) were observed at 2q (43°, 50.5°, and 74.5°) because the Ni–Pd–Au layer was considerably thin. A peak of Au (111) was noted at 2q of approximately 38°.

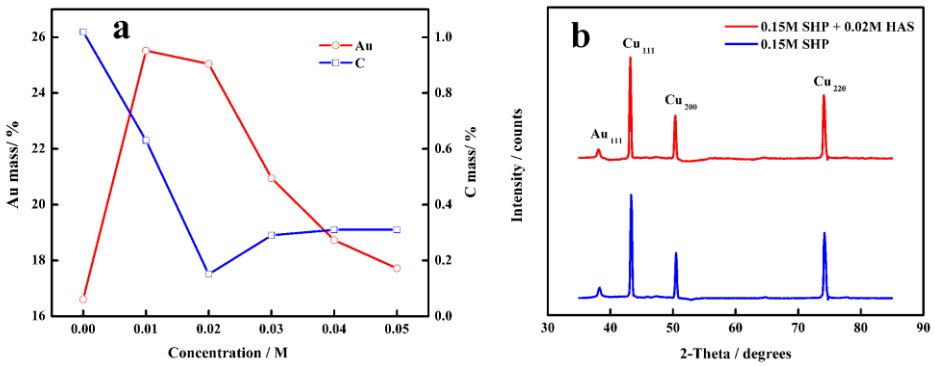

Figure 11. a) Au and O mass of Au surface after 10min electroless plating in EG plating bath different concentrations of HAS, b) XRD patterns of Au layer which deposited with 0.15 M SHP, the mixture of 0.15 M SHP and 0.02 M HAS.

3.8 Corrosion Resistance Study

Figure 12 shows the potentiodynamic polarization curves of different layers in 3.5% NaCl. Table 3 lists the corresponding parameters, including corrosion potential (E_{corr}), corrosion current (I_{corr}), anodic transfer coefficient (β_a), cathodic transfer coefficient (β_c), and polarization resistance (R_p), which were calculated using the CHI electrochemical station.

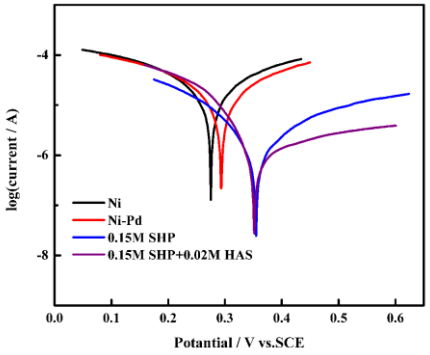

Figure 12. Potentiodynamic polarization curves of copper covered by Ni, Ni-Pd, Ni-Pd-Au which the Au layer deposited in 0.15 M SHP and Ni-Pd-Au which the Au layer deposited in 0.15 M SHP and 0.02 M HAS.

Table 4. Corrosion properties of different Potentiodynamic polarization curves

Sample	E_{corr} (V)	I_{corr} (I)	β_a (V/decade)	β_c (V/decade)	R_p (Ohm)	P(%)
Ni	0.275	2.597×10^{-5}	0.208	0.195	1681	—
Ni-Pd	0.294	1.995×10^{-5}	0.213	0.193	2206	61.72
0.15 M SHP	0.355	1.981×10^{-6}	0.167	0.129	16102	4.30
0.15 M SHP+0.02 M HAS	0.352	2.164×10^{-6}	0.303	0.116	16808	4.26

The total coating porosity (P) was calculated using Equation (III)[38]. The copper was covered with the Ni layer as the substrate, and ΔE denoted the corrosion potential difference between the coating and the substrate.

$$P = \frac{R_{p(substrate)}}{R_{p(coating)}} \times 10^{-|\Delta E/\beta_{a(substrate)}|} \qquad \text{Equation (III)}$$

Figure 12 shows that the corrosion potential had a positive shift and that the corrosion current decreased after EP or EG plating. Furthermore, the presence of HAS decreased the corrosion current. The total coating porosity with the Au layer deposited in the complex reducing agents was the smallest, as shown in Table 3, because HAS smoothened the Au surface and had no negative effect on the Ni/Pd layer.

4. CONCLUSION

To reveal the effects of HAS on electroless gold plating bath and deposition procedure, we investigated the stability of the bath, deposition rate, electrochemistry, surface microtopography, and chemical and phase composition. The results are as follows:

(1) As was the most suitable reducing agent, and HAS did not affect the stability of the Au plating bath. Nevertheless, 0.02 M HAS could accelerate the Au deposition rate by 70% on the Ni–Pd surface.

(2) $Au(CN)_2^-$ was transformed to $Au(C(NH_2)NOH)_2^-$ the addition of HAS, and this reaction affected the deposition rate because the reactivity of the Au atom decreased.

(3) HAS enhanced the charge transfer because of its catalyzed oxidation on the Au surface, resulting in rapid Au deposition after the Ni–Pd surface was covered with the Au layer.

(4) As result of the transformation of the nucleation mechanism, the size of the Au grain increased, and the Au surface became smooth along with HAS at the same deposition time. This micromorphological structure improved the corrosion resistance of the total coating.

In summary, the complex reducing agents overcame the difficulty of Au deposition after the Ni–Pd surface was covered with the Au layer when only SHP was used. The improvement of deposition rate and corrosion resistance is conducive to the enhancement of industrial production efficiency and satisfies the trend of high compactness and high frequency of PCBs.

ACKNOWLEDGMENETS

This work was founded by the Changsha Municipal Science and Technoligy Plan (NO.kq1701077, NO.kq1706063) Green Manufacturing System Integration Project (Green key process system integration for high precision printed circuit boards), the Strategic Emerging Industry Scientific and Technological Research and Major Achievements Transformation Project of Hunan Province (NO.2015GK1046).

References

1. M. Ratzker, A. Pearl, M. Osterman, M. Pecht and G. Milad, *J. Electron. Mater.*, 43 (2014) 3885.
2. P.T. Vianco, *Circuit World*, 25 (1999) 6.
3. S.B. Jung, B.I. Noh, W.S. Hong and J.W. Yoon, *J. Electron. Mater.*, 38 (2009) 902.
4. G. Milad, *Circuit World*, 34 (2009) 4.
5. B.I. Noh, J.B. Lee and S.B. Jung, *Microelectron. Reliab.*, 48 (2008) 652.
6. J. Sudagar, J. Lian and W. Sha, *J.Alloy.Compd.*, 571 (2013) 183.
7. H. Liu, L. Gao, Y. Wang, S. Bi, C. Wang and M. He, *Rsc. Adv.*, 6 (2016) 9656.
8. B. Li, N. Li, G. Luo and D. Tian, *Surf. Coat. Technol.*, 302 (2016) 202.
9. M. Oezkoek, G. Ramos, D. Metzger and H. Roberts, *IEEE Electron. Syst. Technol.*, 2010.

10. H.P. Lima, A. Ourdjini, T.A.A. Bakar and T. Tesfamichael, *Procedia Manuf.*, 2 (2015) 275.
11. W. Wang, A. Choubey, M.H. Azarian and M. Pecht, *J. Electron. Mater*., 38 (29) 815.
12. M. Ramirez, L. Henneken and S. Virtanen, *Appl. Surf. Sci.*, 257 (2011) 6481.
13. A. Chaillot, N. Venet, P.E. Tegehall, J. Hokka and J.L. Lortal, *IEEE Eur. Microelectron. Packag.*, 2013.
14. C.C. Lee, H.Y. Chuang, C.K. Chung and C.R. Kao, *IEEE Microsyst. Packag. Assembly Circuits Technolo.*, 2010.
15. K.P.L. Pun, M.N. Islam, C.W. Cheung and A.H.S. Chan, *J. Mater. Sci. Mater. Electron*., 28 (2017) 12617.
16. Z. Hai, J. Zhang, C. Shen, E.K. Snipes, M.J. Bozack, J.L. Evans and J.C. Suhling, *J. Mechatron.*, 2 (2014) 100.
17. B. Li, N. Li, D. Li and Y. Wang, *Rsc. Adv.*, 6 (2016) 34797.
18. C.D. lacovangelo, *J. Electrochem. Soc.*, 138 (1991) 976.
19. M. Kato and Y. Okinaka, *Gold. Bull.*, 37 (2004) 37.
20. Y. Yasutake and K. Kono, *Appl. Phys. Lett.*, 91 (2007) 203107.
21. S. Dimitrijević, M. Rajčić-Vujasinović and V. Trujić, *J. Electrochem. Sci.*, 8 (2013) 6620.
22. V.D. Meerakker, *J. Appl. Electrochem.*, 11 (1981) 395.
23. E.F.D. Monlevade and W. Peng, *J. Electron. Mater.*, 36 (2007) 783.
24. W. Machu and S. EI-Gendi, *Metalloberflache*, 13 (1959) 97.
25. A. Brenner and G.E. Riddell, *Proc. Am. Electropl. Soc.*, 33 (1946) 16.
26. T. Homma, I. Komatsu, A. Tamaki, H. Nakai and T. Osaka, *Electrochim. Acta*, 47 (2001) 47.
27. X. Tang, J. Wang, C. Wang and B. Shen, *Surf. Coat. Technol.*, 206 (2011) 1382.
28. P.P. Mardilovich, Y. She, Y.H. Ma and M.H. Rei, *Aiche. J*., 44 (1998) 310.
29. W. Ping, Y. Song, Y. Zhao and A. Fan, *Talant*, 103 (2013) 392.
30. L. Yao, X. Yu, Y. Zhao and A. Fan, *Anal. Methods*, 7 (2015) 8786.
31. M.R. Rahman, F.S. Saleh, T. Okajima and T. Ohsaka, *Langmuir.*, 27 (2011) 5216.
32. S.K. Kang, Y. Kim, M.S. Hahn, I. Choi, J. Lee and J. Yi, *Curr. Appl. Phys*., 6 (2006) e114.
33. J.K. Young, A.V. Nixon, A. Satyanarayan and R.A. Drezek, *Part. Part. Syst. Charact.*, 31 (2014) 948.
34. N.A. Dogan, Y. Hong, E. Ozdemir and C.T. Yavuz, *ACS Sustainable Chem. Eng.*, 7 (2019) 123.
35. M. Raja, R.R. Muhamed, S. Muthu and M. Suresh, *J. Mol. Struct.*, 1141 (2017) 284.
36. A. Tamaki, T. Shimada and H. Nakai, *Electrochem*., 75 (2007) 45.
37. Z. Lin, B. Xie, J. Chen, J. Sun and G. Chen, *J. Electroanal. Chem.*, 633 (2009) 207.
38. Y. Wang, H. Liu, S. Bi, M. He, C. Wang and L. Cao, *RSC advances*, 6 (2016) 9656.